5 Theoretical study of photoabsorption spectroscopy of carbon chains. C_{15}

5.1 Introduction

DIBs are absorption features seen in the spectra of reddened stars through diffuse interstellar clouds [1]. Over 400 bands are seen, in ultraviolet, visible and infrared wavelengths. Identification of carriers of DIBs has been a long standing and unresolved issue in the astrophysical spectroscopy. The diffuse structure of these bands is attributed to the very short life times of the excited electronic states of the carrier molecule [2]. Douglas in his seminal paper, suggested that the bare carbon chains C_n, where n may lie in the range 5-15 [3] could show spectroscopic features consistent with the DIBs. The first spectroscopic detection of C_3 in comets in 1881 [4] triggered curiosity among the astronomers, chemists and physicists to further investigate structure and spectroscopy of carbon chains.

Since then many experimental and theoretical studies were reported on the structure of anionic, neutral and cationic bare carbon clusters. Here we refer to two reviews on the rich history of carbon cluster chemistry by Weltner [5] and Orden [6]. Carbon clusters smaller than C_{10} possess low-energy linear structures. Cumulenic bonding (:C=C–C=C:), with nearly equivalent bond lengths, as opposed to acetylenic bonding, (.C≡C-C—C≡C) with alternating bond lengths, was predicted to be the preferred bonding configuration. Linear chains containing odd number of carbon atoms were thought to possess $^1\Sigma_g^+$ ground electronic states, whereas the ground states were $^3\Sigma_g^-$ for the chains with even number of carbon atoms. Clusters larger than C_{10} were believed to occur as monocyclic rings, due to the reduction in angle strain of the larger rings and the added stability arising from an additional C-C bond. Despite this, the cyclic isomers of the neutral clusters reported to be difficult to detect and characterize spectroscopically, and it is the linear isomers that are observed in the vast majority of experimental studies. This is the case even for clusters as large as C_{15}.

The neutral and anions of bare carbon chains are studied with various spectroscopic techniques ranging from pulsed and continuous-wave CRD, R2C2PI, LIF, trapped ion photofragmentation, and electron photodetachment processes during the past decade [7–11] to examine the conjecture of Douglas. It was proved from the study of Maier *et al.* that bare carbon chains C_n upto n=12 can not be carrier for DIBs. The following criteria are formulated by the latter authors for a species to have to be a potential DIB carrier: "(a) absorptions in the 400-800 nm range, (b) oscillator strength f values in the 1-10 range, and (c) an excited electronic-state lifetime longer than a few picoseconds so

Table 5.1: VEEs (in eV) of low-lying excited singlet electronic states calculated at the equilibrium geometry of S_0 state of C_{15}.

Symbol	Excitation energy (eV)	f
$S_1{}^1\Delta_u$	0.6701	0.00
$S_2{}^1\Sigma_u^-$	0.7461	0.00
$S_3{}^1\Sigma_g^-$	2.1277	0.00
$S_4{}^1\Delta_g$	2.1431	0.00
$S_5{}^1\Pi_g$	3.1081	0.00
$S_6{}^1\Pi_u$	3.1097	0.01
$S_7{}^1\Sigma_u^+$	3.2729	12.97
$S_8{}^1\Sigma_u^-$	3.4325	0.00
$S_9{}^1\Sigma_g^-$	3.4485	0.00
$S_{10}{}^1\Delta_g$	3.4800	0.00
$S_{11}{}^1\Delta_u$	3.5148	0.00
$S_{12}{}^1\Sigma_g^+$	3.6132	0.00

that intramolecular broadening would still be compatible with the typical half-widths of the narrower DIBs (i.e., a few wave numbers)" [10]. The longer chains with an odd number of carbon atoms of the length 15, 17, 19 and 21 are expected to satisfy the first two criteria because their transitions are in the 400-800 nm range and their f values scale with the chain length. It remains to be seen by doing nuclear dynamics study, whether the excited electronic state $S_7{}^1\Sigma_u^+$ has a lifetime longer than a few picoseconds to satisfy the third condition listed above.

The low-lying electronic excited states of C_{15} and their oscillator strengths are tabulated in Table 5.1. *Ab initio* calculation of the excited states are described in Section 5.2. As can be seen from the table, the electronic states are very closely spaced, infact 18 electronic states (including degeneracy) appear within 4.0 eV, ideally which need to be studied, for a correct description of the nuclear dynamics. While, consideration all the electronic states would be much appreciated, both the *ab initio* electronic structure calculations and nuclear dynamics simulations would be computationally very challenging and difficult. While the first one (*ab initio* calculations) can be feasible with relatively less expensive yet reliable methods such as equation of motion coupled cluster with single and double excitations (eom-CCSD), the later (nuclear dynamics) with all the 18 electronic states appears to be impossible to study. As our study, primarily focuses on the life time of $S_7{}^1\Sigma_u^+$ electronic state of C_{15}, we retain only those electronic states which couple to $S_7{}^1\Sigma_u^+$ electronic state according to the vibronic coupling selection rules given in Section 5.3. From the selection rules, it can be seen that only $S_5{}^1\Pi_g$, $S_6{}^1\Pi_u$ and $S_{12}{}^1\Sigma_g^+$ electronic states couple to $S_7{}^1\Sigma_u^+$ electronic state.

In this chapter, such study of the nuclear dynamics in the $S_5{}^1\Pi_g$, $S_6{}^1\Pi_u$, $S_7{}^1\Sigma_u^+$ and $S_{12}{}^1\Sigma_g^+$ coupled electronic states of C_{15} carbon chain, by doing rigorous electronic structure calculations is presented. The well celebrated BO approximation fails [18–22]

when two electronic states happen to be degenerate or near degenerate. The reason for such breakdown is the non-adiabatic coupling operator behaves singularly at degeneracy. Familiar examples for such breakdown of BO approximation are JT [23] and RT [24] effects. The RT has been considered as the driving force behind bending instability of linear molecules in degenerate states [31]. Upon bending the molecule, an additional dipole moment is set up in the molecular plane which lifts the electronic degeneracy. In contrast to this, it was proved very recently that the RT effect in fact produces just a splitting of the degenerate term, but not any bending instability. All instabilities and distortions of linear molecules arise due to the mixing with appropriate excited electronic states which is called as the PJT effect [32].

The RT effect in triatomic molecules is extensively studied theoretically by perturbative treatment of the Hamiltonian when expanded in a Taylor series around the linear configuration [24–27]. While there are plethora of studies on the triatomic RT effect, studies on linear polyatomic molecules with atoms more than three, are very less. To the best of our knowledge carbon chains of upto 6 atom length were theoretically studied by including the RT [29, 30] effect. However perturbation theory is known to fail in strong coupling case and when the interacting states are very closely spaced. A quasi-diabatic-Hamiltonian is proposed by Köppel *et al.* to avoid the perturbative treatment of the RT [20, 28] intersections. On rigorous study, this model diabatic Hamiltonian is wide accepted by the scientific community.

This chapter is organized as follows. The details of electronic structure calculations are given in Sec 5.2. The vibronic Hamiltonian is derived in Sec 5.3 by considering the group theoretical approach. The topography of the adiabatic potential energy surfaces are presented in Sec. 5.4. While the theoretical absorption spectrum is discussed in Sec. 5.5, the internal conversion dynamics is discussed in Sec. 5.6.

5.2 Electronic structure calculations

The reference equilibrium geometry of the electronic ground state $S_0{}^1\Sigma_g^+$ of C_{15} is optimized by the B3LYP method employing the cc-pVDZ basis set of Dunning [35]. The geometry parameters are tabulated in Table 5.2 along with the literature data. Harmonic frequency (ω_i) of the vibrational modes of C_{15} is calculated by diagonalizing the kinematic and *ab initio* force constant matrix of the reference equilibrium structure. These vibrational frequencies (in eV units) are listed in the third column of Table 5.3. The mass-weighted normal coordinates of the vibrational modes are calculated from the eigenvectors of the force constant matrix. These are then transformed into their dimensionless form ($\mathbf{Q}_i$) by multiplying with $\sqrt{\omega}_i$ (in a_0) [36]. The fundamental vibrational modes of C_{15} decompose into thirteen degenerate and fourteen non degenerate symmetry species of the $D_{\infty h}$ symmetry point group. They transform into the following IREPs of this symmetry point group:

$$\Gamma = 7\sigma_g(\nu_1 - \nu_7) \oplus 7\sigma_u(\nu_8 - \nu_{14}) \oplus 6\pi_g(\nu_{15} - \nu_{20}) \oplus 7\pi_u(\nu_{21} - \nu_{27}). \quad (5.1)$$

Table 5.2: Optimized equilibrium geometry parameters of the electronic ground state of C_{15}. The results available from the literature [33] are also included in the table for comparison. All units are given in

Parameter	B3LYP/cc-pVDZ [33]	B3LYP/cc-pVDZ This work	MP2/cc-pVDZ This work
R_{12}	1.29	1.29	1.32
R_{23}	1.30	1.30	1.31
R_{34}	1.28	1.27	1.29
R_{45}	1.29	1.29	1.30
R_{56}	1.28	1.28	1.30
R_{67}	1.29	1.29	1.30
R_{78}	1.28	1.28	1.30

The geometry optimization and calculation of the normal modes of vibrations are performed using G03 suit of *ab initio* programs [37]. Adiabatic energies of the low-lying singlet electronic states of C_{15} are calculated *ab initio* along the dimensionless normal coordinates of the 27 (altogether) vibrational degrees of freedom. The VEEs of these electronic states are calculated for $Q_i = \pm 0.10$ and in the range -3.0 to $+3.0$ with an increment 0.25, along i^{th} vibrational mode (keeping others at their equilibrium value) using the EOM-CCSD method as implemented in MOLPRO program package [38]. The excited state symbol, excitation energy and oscillator strength are given in Table 5.1.

5.3 Vibronic Hamiltonian

In this section we construct a Hamiltonian describing the vibronic interactions of $S_5{}^1\Pi_g$, $S_6{}^1\Pi_u$, $S_7{}^1\Sigma_u^+$ and $S_{12}{}^1\Sigma_g^+$ excited electronic states of C_{15} cluster in terms of the normal displacement coordinates of the reference electronic ground state of respective carbon chain, in accordance with the symmetry selection rules. The Hamiltonian is constructed in a diabatic electronic basis [20]. The molecular Hamiltonian in linear vibronic coupling scheme for E_{1g}, E_{1u}, A_{2u} and A_{1g} interacting electronic manifold for Benzene and HFBz are derived thoroughly by Köppel *et al.* and Mahapatra *et al.* [39–41]. In the analogous manner, the molecular Hamiltonian for interacting manifold of excited electronic states of odd numbered carbon chains can be written.

The first-order coupling within (intra) and between (inter) electronic states is governed by the selection rules; $(\Gamma_i)^2 \supset (\Gamma_{\sigma_g^+})$ and $\Gamma_i \otimes \Gamma_j \supset \Gamma_x$, respectively [20]. The symbol, Γ represents the IREP, i and j are the electronic state indices, σ_g^+ represents the totally symmetric vibrational mode and the symbol, x, represents the symmetry of the vibrational mode that transforms according to, $\Gamma_i \otimes \Gamma_x \otimes \Gamma_j \supset \Sigma_g^+$. Now for the degenerate, $S_5{}^1\Pi_g$ and $S_6{}^1\Pi_u$ electronic states the symmetrized direct product transforms into, $(\Pi_g)^2 = (\Pi_u)^2 = \Sigma_g^+ + \Delta_g$. While the vibrational modes of σ_g^+ symmetry can not split the electronic degeneracy (are condon active), and the lack of δ_g modes of symmetry that can lift this electronic degeneracy makes first order RT coupling vanish.

But the electronic degeneracy of Π_g and Π_u states is lifted by the π_g and π_u modes in second order. For the rest of the off-diagonal elements of the Hamiltonian written below the following symmetry rules apply. With the given symmetry representation of the electronic states and the vibrational modes [in Eq. (5.1)] of C_{15} the following rules can be derived from the character table of the $D_{\infty h}$ symmetry point group.

$$\begin{aligned}
\Pi_g \otimes \Pi_u &= \delta_u + \sigma_u^- + \sigma_u^+(8-14),\\
\Pi_g \otimes \Sigma_u^+ &= \pi_u(21-27),\\
\Pi_g \otimes \Sigma_g^+ &= \pi_g(15-20),\\
\Pi_u \otimes \Sigma_u^+ &= \pi_g(15-20),\\
\Pi_u \otimes \Sigma_g^+ &= \pi_u(21-27),\\
\Sigma_u^+ \otimes \Sigma_g^+ &= \sigma_u^+(8-14),
\end{aligned}$$

Where the numbers in the parentheses in the right hand side indicates the vibrational mode number given in Eq. 5.1. The relative sign of various elements of the Hamiltonian is determined by explicitly checking the invariance of the Hamiltonian with respect to the symmetry operations of the D_{6h} point group, following similar works on benzene and cyclopropane radical cation [39–41]. With these considerations the vibronic Hamiltonian can be written as

$$\mathcal{H} = \mathcal{H}_0 \mathbf{1_6} + \mathcal{W}, \tag{5.2a}$$

where

$$\mathcal{W} = \begin{bmatrix}
\mathcal{E}^5 + \mathcal{U}^{5x} & \sum\limits_{i\in\pi_u,\pi_g} \eta_i^{3x,3y} Q_{ix}Q_{iy} & \sum\limits_{i\in\sigma_u^+} \lambda_i^{3x,4x} Q_i & \sum\limits_{i\in\sigma_u^-} \lambda_i^{3x,4y} Q_i & \sum\limits_{i\in\pi_u} \lambda_i^{3x,7} Q_{ix} & \sum\limits_{i\in\pi_x} \lambda_i^{3x,8} Q_{ix} \\
 & \mathcal{E}^3 + \mathcal{U}^{3y} & \sum\limits_{i\in\sigma_u^-} \lambda_i^{3y,4x} Q_{iy} & \sum\limits_{i\in\sigma_u^+} \lambda_i^{3y,4y} Q_i & \sum\limits_{i\in\pi_u} \lambda_i^{3y,7} Q_{iy} & \sum\limits_{i\in\pi_g} \lambda_i^{3y,8} Q_{iy} \\
 & & \mathcal{E}^4 + \mathcal{U}^{4x} & \sum\limits_{i\in\pi_u,\pi_g} \eta_i^{4x,4y} Q_{ix}Q_{iy} & \sum\limits_{i\in\pi_g} \lambda_i^{4x,7} Q_{ix} & \sum\limits_{i\in\pi_g} \lambda_i^{4x,7} Q_{ix} \\
 & & & \mathcal{E}^{4y} + \mathcal{U}^{4y} & \sum\limits_{i\in\pi_g} \lambda_i^{4y,7} Q_{iy} & \sum\limits_{i\in\pi_g} \lambda_i^{4y,8} Q_{iy} \\
 & & h.c. & & \mathcal{E}^7 + \mathcal{U}^7 & \sum\limits_{i\in\sigma_u} \lambda_i^{7,8} Q_i \\
 & & & & & \mathcal{E}^8 + \mathcal{U}^8
\end{bmatrix} \tag{5.2b}$$

In the above, $\mathcal{H}_0 = \mathcal{T}_N + \mathcal{V}_0$, represents the Hamiltonian (assumed to be harmonic) of the reference electronic ground (S_0) state of C_{15} with

$$\mathcal{T}_N = -\frac{1}{2}\sum_{i\ \in\ \sigma_g^+,\ \sigma_u^-} \omega_i \frac{\partial^2}{\partial Q_i^2} - \frac{1}{2}\sum_{i\ \in\ \pi_g,\ \pi_u} \omega_i \left(\frac{\partial^2}{\partial Q_{ix}^2} + \frac{\partial^2}{\partial Q_{iy}^2}\right), \tag{5.3}$$

and

$$\mathcal{V}_0 = \frac{1}{2} \sum_{i \in \sigma_g^+,\, \sigma_u^-} \omega_i Q_i^2 + \frac{1}{2} \sum_{i \in \pi_g,\, \pi_u} \omega_i \left(Q_{ix}^2 + Q_{iy}^2 \right). \tag{5.4}$$

The quantity $\mathbf{1_6}$ is a 6×6 diagonal unit matrix. The nondiagonal matrix Hamiltonian in Eq. (5.2b) describes the PESs of the excited electronic states of C_{15} and their coupling surfaces. The quantity $\mathcal{E}^j$ in this matrix is the VEE of the j^{th} electronic state. The elements of this matrix are expanded in a standard Taylor series around the reference equilibrium geometry at, $\mathbf{Q} = \mathbf{0}$, in the following way

$$\mathcal{U}^j = \sum_{i \in \sigma_g^+} \kappa_i^j Q_i + \frac{1}{2} \sum_{i \in \sigma_g^+,\, \sigma_u^-} \gamma_i^j Q_i^2 + \frac{1}{2} \sum_{i \in \pi_g,\, \pi_u} [\gamma_i^j (Q_{ix}^2 + Q_{iy}^2)] \tag{5.5a}$$

$$\mathcal{U}^{jx/jy} = \sum_{i \in \sigma_g^+} \kappa_i^j Q_i \pm \sum_{i \in \pi_g,\, \pi_u} \eta_i^j (Q_{ix}^2 - Q_{iy}^2) + \frac{1}{2} \sum_{i \in \sigma_g^+,\, \sigma_u^-} \gamma_i^j Q_i^2 + \frac{1}{2} \sum_{i \in \pi_g,\, \pi_u} [\gamma_i^j (Q_{ix}^2 + Q_{iy}^2)];$$
$$j \in 1 \text{ and } 2. \tag{5.5b}$$

In above equations the two components of the degenerate states and modes are labeled with x/y. The quantity κ_i^j and η_i^j represents the linear intrastate and quadratic RT coupling parameters [20] for the symmetric (σ_g^+) and degenerate (π_g, π_u) vibrational modes, respectively, for the j^{th} electronic state. The first-order PJT coupling parameter of the i^{th} vibrational mode between the electronic states j and k is given by λ_i^{j-k} and γ_i^j are the second-order parameters of the i^{th} vibrational mode for the j^{th} electronic state. The summations run over the normal modes of vibration of specified symmetry in the index. The + and - sign in Eq. (5.5b) is applicable to the x and y components of the degenerate state, respectively. The VEEs calculated in Sec. 5.2 are fitted to the adiabatic counterpart of diabatic electronic Hamiltonian of Eq. 5.2 by a least squares procedure to estimate the parameters of the Hamiltonian defined above. The estimated parameters along the relevant vibrational modes are given in Tables 5.3 and 5.4. A careful inspection of the coupling parameters suggests that not all 40 vibrational modes play significant role in the nuclear dynamics on the electronic states of C_n cluster considered in this chapter. Therefore, only the relevant modes having significant coupling strengths are retained in the nuclear dynamics study presented below.

Table 5.3: *Ab initio* calculated linear and quadratic coupling constants for the $S_5{}^1\Pi_g$, $S_6{}^1\Pi_u$, $S_7{}^1\Sigma_u^+$ and $S_{12}{}^1\Sigma_g^+$ electronic states of C_{15} cluster. All data are given in the eV unit.

Symm	Mode	Freq	κ_i or η_i	γ_i	κ_i or η_i	γ_i	κ_i	γ_i	κ_i	γ_i
			$S_5{}^1\Pi_g$		$S_6{}^1\Pi_u$		$S_7{}^1\Sigma_u^+$		$S_{12}{}^1\Sigma_g^+$	
σ_g^+	ν_1	0.2780	0.0956 (0.06)	-0.0110	0.0956 (0.06)	-0.0110	-0.0068 (0.00)	-0.0147	-0.0168 (0.00)	-0.0034
	ν_2	0.2748	0.2381 (0.37)	0.0397	0.2372 (0.37)	0.0409	0.0356 (0.01)	-0.0441	-0.0276 (0.01)	-0.0478
	ν_3	0.2549	0.1529 (0.18)	-0.0112	0.1523 (0.18)	-0.0119	0.0028 (0.00)	-0.0038	-0.0275 (0.01)	-0.0045
	ν_4	0.2175	-0.0854 (0.08)	-0.0038	-0.0851 (0.08)	-0.0038	0.0017 (0.00)	-0.0029	0.0192 (0.00)	-0.0020
	ν_5	0.1622	0.0483 (0.04)	-0.0006	0.0481 (0.04)	-0.0005	-0.0044 (0.00)	-0.0017	-0.0156 (0.01)	-0.0014
	ν_6	0.1014	0.0171 (0.01)	0.0002	0.0170 (0.01)	0.0002	-0.0077 (0.00)	-0.0012	-0.0190 (0.02)	-0.0004
	ν_7	0.0349	-0.0026 (0.00)	0.0001	-0.0026 (0.00)	0.0001	-0.0272 (0.30)	0.0001	-0.0221 (0.20)	0.0002
σ_u^+	ν_8	0.2802	-	-0.0153	-	-0.0151	-	-0.0193	-	-0.0080
	ν_9	0.2687	-	-0.0123	-	-0.0125		-0.0120	-	-0.0165
	ν_{10}	0.2481	-	-0.1746	-	-0.0186	-	-0.4697	-	0.0607
	ν_{11}	0.2386	-	-0.0352	-	0.0032	-	-0.0641	-	0.0150
	ν_{12}	0.1903	-	-0.0013	-	-0.0015	-	-0.0027	-	-0.0016
	ν_{13}	0.1325	-	-0.0001	-	-0.0001	-	-0.0014	-	-0.0013
	ν_{14}	0.0688	-	-0.0008	-	0.0012	-	-0.0020	-	0.0007
π_g	ν_{15}	0.0943	0.0095 (0.01)	-0.0096	-0.0074 (0.00)	-0.0137	-	-0.0015	-	-0.0057
	ν_{16}	0.0735	0.0083 (0.01)	-0.0055	-0.0069 (0.00)	-0.0101	-	-0.0049	-	-0.0073
	ν_{17}	0.0569	0.0078 (0.01)	-0.0061	-0.0076 (0.01)	-0.0072	-	-0.0073	-	-0.0094
	ν_{18}	0.0341	0.0007 (0.00)	0.0266	-0.0007 (0.00)	0.0305	-	-0.0028	-	-0.0021
	ν_{19}	0.0190	0.0004 (0.00)	0.0205	-0.0004 (0.00)	0.0209	-	-0.0046	-	-0.0060
	ν_{20}	0.0064	0.0003 (0.00)	0.0130	-0.0003 (0.00)	0.0129	-	-0.0054	-	-0.0073
π_u	ν_{21}	0.1063	0.0083 (0.00)	-0.0067	-0.0083 (0.00)	-0.0108	-	-0.0053	-	-0.0000
	ν_{22}	0.0838	0.0083 (0.01)	-0.0108	-0.0082 (0.01)	-0.0090	-	-0.0033	-	0.0000
	ν_{23}	0.0648	0.0077 (0.01)	-0.0074	-0.0077 (0.01)	-0.0054	-	-0.0061	-	-0.0091
	ν_{24}	0.0397	0.0017 (0.00)	0.0133	-0.0018 (0.00)	0.0195	-	-0.0072	-	-0.0031
	ν_{25}	0.0268	0.0014 (0.00)	0.0250	-0.0013 (0.00)	0.0267	-	-0.0039	-	-0.0057
	ν_{26}	0.0121	0.0007 (0.00)	0.0164	-0.0007 (0.00)	0.0165	-	-0.0049	-	-0.0065
	ν_{27}	0.0023	0.0001 (0.00)	0.0099	-0.0001 (0.00)	0.0098	-	-0.0070	-	-0.0090

Table 5.4: Interstate coupling parameters (in eV) of the vibronic Hamiltonian of Eq. 5.2 for the $S_5{}^1\Pi_g$, $S_6{}^1\Pi_u$, $S_7{}^1\Sigma_u^+$ and $S_{12}{}^1\Sigma_g^+$ electronic states of C_{15} cluster estimated from the *ab initio* electronic structure results (see text for details).

Mode	$\lambda_i^{1,2}$	$\lambda_i^{1,3}$	$\lambda_i^{1,4}$	$\lambda_i^{2,3}$	$\lambda_i^{2,4}$	$\lambda_i^{3,4}$
ν_8	0.1439 (0.13)	-	-	-	-	-
ν_9	0.1229 (0.10)	-	-	-	-	-
ν_{10}	0.1531 (0.20)	-	-	-	-	0.2227 (0.40)
ν_{11}	0.1653 (0.23)	-	-	-	-	-
ν_{12}	0.0662 (0.06)	-	-	-	-	0.0112 (0.00)
ν_{13}	0.0341 (0.03)	-	-	-	-	0.0039 (0.00)
ν_{14}	0.0058 (0.00)	-	-	-	-	0.0159 (0.03)
ν_{15}	-	-	0.0331 (0.06)	-	-	-
ν_{16}	-	-	0.0278 (0.07)	0.0190 (0.03)	-	-
ν_{17}	-	-	0.0234 (0.09)	-	-	-
ν_{18}	-	-	-	-	-	-
ν_{19}	-	-	-	-	-	-
ν_{20}	-	-	-	-	-	-
ν_{21}	-	0.0206 (0.02)	-	-	-	-
ν_{22}	-	0.0257 (0.20)	-	-	-	-
ν_{23}	-	0.0183 (0.04)	-	-	0.0206 (0.05)	-
ν_{24}	-	-	-	-	-	-
ν_{25}	-	-	-	-	-	-
ν_{26}	-	-	-	-	-	-
ν_{27}	-	-	-	-	-	-

5.4 Adiabatic potential energy surfaces

In this section we examine the topography of the adiabatic PESs of the four excited singlet electronic states $S_5{}^1\Pi_g$, $S_6{}^1\Pi_u$, $S_7{}^1\Sigma_u^+$ and $S_{12}{}^1\Sigma_g^+$ of C_{15} obtained by diagonalizing the electronic Hamiltonian of the diabatic model developed above. The nonradiative decay of the diabatic population of the $S_7{}^1\Sigma_u^+$ electronic state is calculated and found to depend strongly on the topography of the PESs.

According to the selection rules, given in Sec 5.3, the totally symmetric modes ν_1-ν_7 of C_{15} cannot split the degeneracy of $S_5{}^1\Pi_g$ and $S_6{}^1\Pi_u$ electronic states, while the degenerate bending π_g and π_u modes split the degeneracy of $S_5{}^1\Pi_g$ and $S_6{}^1\Pi_u$ electronic state. One dimensional cuts of the potential energy hypersurfaces of C_{15} are viewed along the given totally symmetric modes (σ_g^+) vibrational mode keeping others at their equilibrium values at, $\mathbf{Q}$=0, are shown in panels (a-g) of Fig. 5.1. In the figure the solid curves represent the adiabatic potential energy functions obtained from the model developed in Sec 5.3 and the points superimposed on them are obtained from *ab initio* quantum chemical calculations discussed in Sec. 5.2. It can be seen from Fig. 5.1 that the *ab initio* energies are very well reproduced by the model.

The energetic minimum of the seam of various CIs and the minimum of the upper adiabatic electronic states are estimated. The resulting data are collected in Table 5.5. The diagonal entries in this table are the energy at the minimum of a state. Whereas, the off-diagonal entries represent the minimum of the seam of CIs. The electronic states S_5 and S_6 are almost degenerate, they are just separated by $\sim$ 0.002 eV from each other. The minimum of S_5 -S_6 intersections is just $\sim$0.28 above the minimum of the upper adiabatic S_6 electronic state. From Table 5.4 it can be seen that interstate coupling between these states is moderately strong along ν_{10} and ν_{11} normal modes of vibrations of symmetry σ_u^+. Similarly the minimum of S_5 -S_7 CIs occurs just $\sim$0.04 eV above the minimum of S_7 electronic state and coupling between these states is facilitated by π_g modes with a strong coupling along ν_{11}. Hence the right wing of S_5 absorption band and the left wing of S_6 and S_7 absorption bands are expected to be strongly perturbed by the S_5 -S_6 and S_5 -S_7 interstate couplings, respectively. Similarly, the minimum of S_5 -S_{12} CIs is $\sim$0.14 eV above the minimum of S_5 electronic state. The interstate coupling between them is negligible. So, the non-adiabatic interactions between them can be safely ignored. As can be seen from the Table 5.5, the minimum of S_6 is just $\sim$0.04, $\sim$0.14 eV below it's CIs with the S_7 and S_{12} electronic states, respectively. The interstate coupling between S_6 -S_7 and S_6 -S_{12} electronic states is negligible (*cf.* Table 5.4). The minimum of S_7 -S_{12} CIs is $\sim$1.81 eV above the minimum of the upper adiabatic sheet of the S_{12} state. This separation is relatively high when compared to the remaining energetic positions discussed above. However, the strong coupling between S_7 -S_{12} makes the nonadiabatic interactions stronger in these coupled electronic states.

The RT effect lifts the degeneracy of S_5 and S_6 electronic states when the molecule is distorted along π_g (ν_{15}-ν_{20}) and π_u (ν_{21}-ν_{27}) normal coordinates of vibration in second order. Now let us consider the topography of S_5 and S_6 electronic states. The Hamiltonian for degenerate electronic state (S_5 or S_6) including only the π_g modes is given

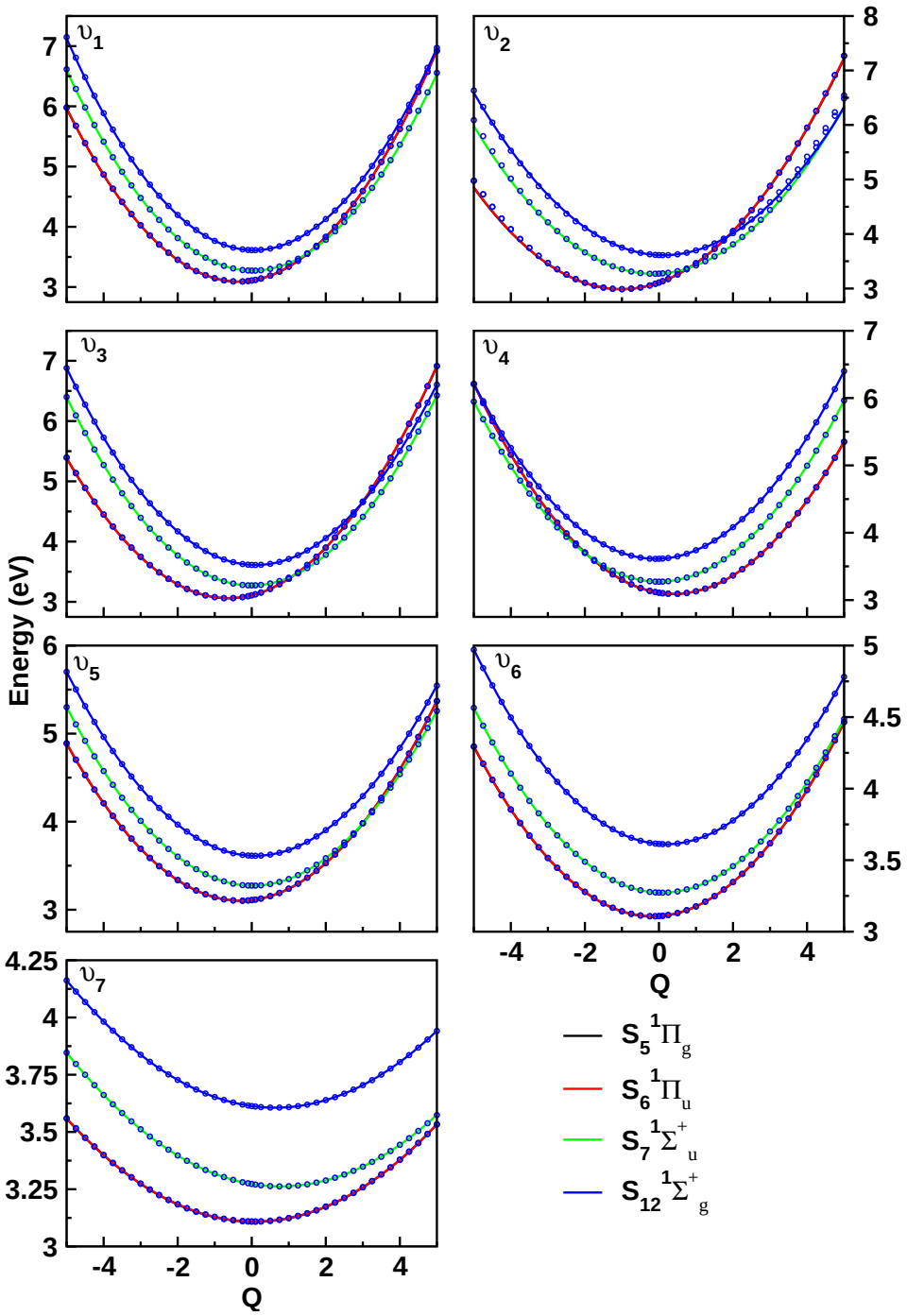

Figure 5.1: Adiabatic potential energies of the low-lying excited singlet electronic states of C_{15}, along the normal coordinates of totally symmetric vibrational modes. The potential energies obtained from the present vibronic model are shown by the solid lines and the computed *ab initio* energies are shown by the circles.

Table 5.5: Estimated equilibrium minimum (diagonal entries) and minimum of the seam of various CIs (off-diagonal entries) of the electronic states of C_{15} within a quadratic coupling model. All quantities are given in eV.

	$S_5\,^1\Pi_g$	$S_6\,^1\Pi_u$	$S_7\,^1\Sigma_u^+$	$S_{12}\,^1\Sigma_g^+$
$S_5\,^1\Pi_g$	2.89	3.17	3.30	3.74
$S_6\,^1\Pi_u$	-	2.89	3.30	3.74
$S_7\,^1\Sigma_u^+$	-	-	3.26	5.41
$S_{12}\,^1\Sigma_g^+$	-	-	-	3.60

as

$$\mathcal{H} = \begin{bmatrix} E + \frac{1}{2}(\omega+\gamma)(Q_x^2+Q_y^2) + \frac{1}{2}\eta(Q_x^2-Q_y^2) & \eta Q_x Q_y \\ \eta Q_x Q_y & E_1 + \frac{1}{2}(\omega+\gamma)(Q_x^2+Q_y^2) - \frac{1}{2}\eta(Q_x^2-Q_y^2) \end{bmatrix}$$

Diagonalization the above diabatic Hamiltonian results adiabatic PESs

$$V_{\pm} = E + \frac{1}{2}(\omega+\gamma-\eta)(Q_x^2+Q_y^2)$$

Minimization of V_- with respect to Q_x suggest V_- is minimum or maximum (at Q_x=0) depending on whether the quantity $\omega+\gamma-\eta$ is greater or less than zero. From the above expression, it is quite clear that RT effect can not induce a new minimum for the degenerate electronic state (S_5 or S_6) and it can not explain the bent geometries of the excited states of the linear polyatomic molecules unless strong anharmonicity terms are presented in the PESs [32].

To explain the bent geometries of the excited states, one has to resort to $\Pi-\Sigma$ coupling mechanism. To obtain the adiabatic PES of C_{15} along π_g mode, one needs to diagonalize the Hamiltonian 5.2b containing only the x components of π_g mode. The analytical expression for the resultant PESs are given in Eq. 5.7 and are plotted in Fig. 5.2. Similarly the one dimensional cuts of the adiabatic PESs of electronic states of C_{15} along π_u vibrational normal coordinates are given in Eq. 5.8 and are plotted in Fig. 5.3.

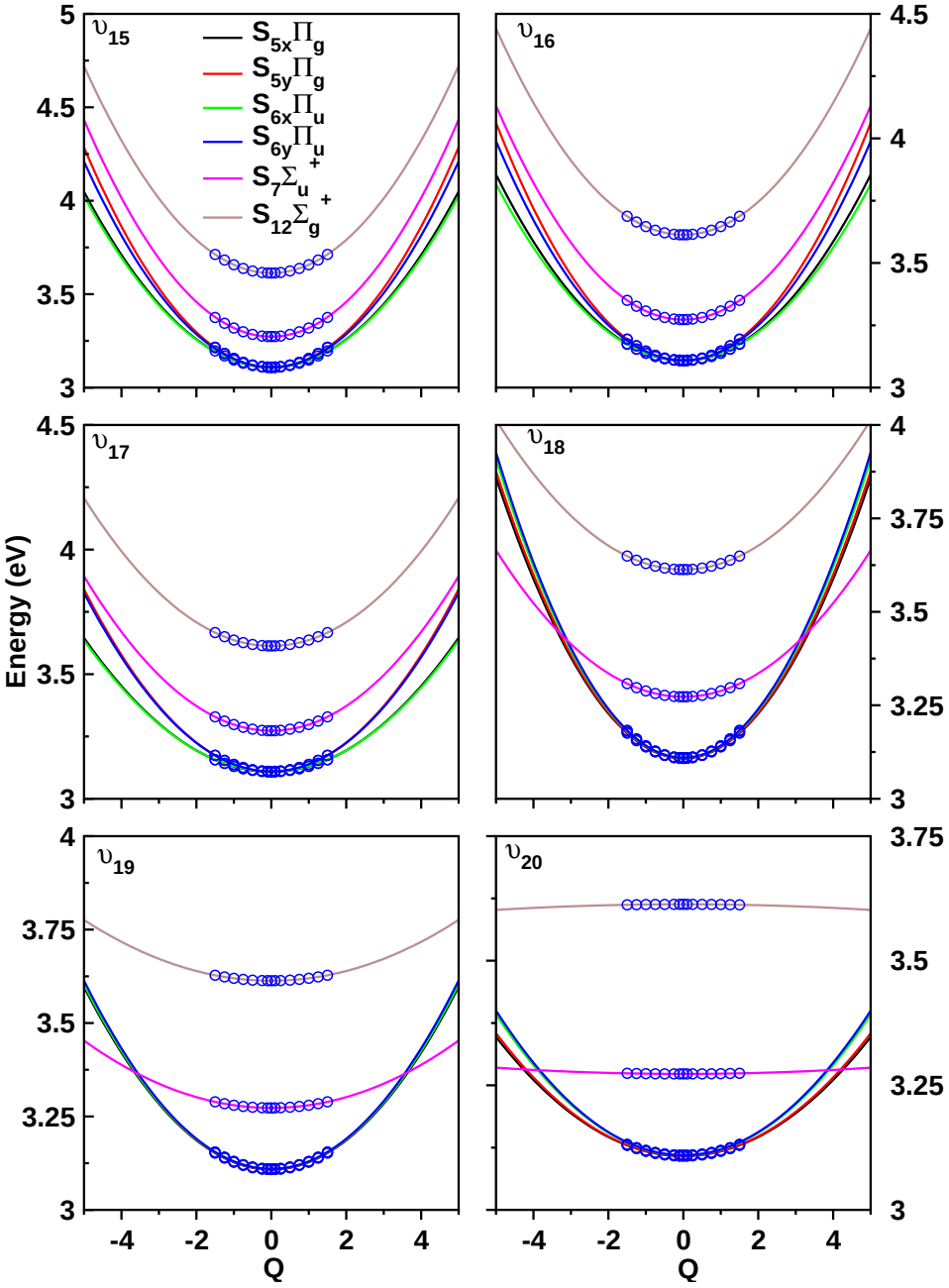

Figure 5.2: Adiabatic potential energies of S_5 , S_6 , S_7 and S_{12} electronic states of C_{15}, along the normal coordinates of degenerate bending π_g vibrational modes. The potential energies obtained from the present vibronic model are shown by the solid lines and the computed *ab initio* energies are shown by the circles.

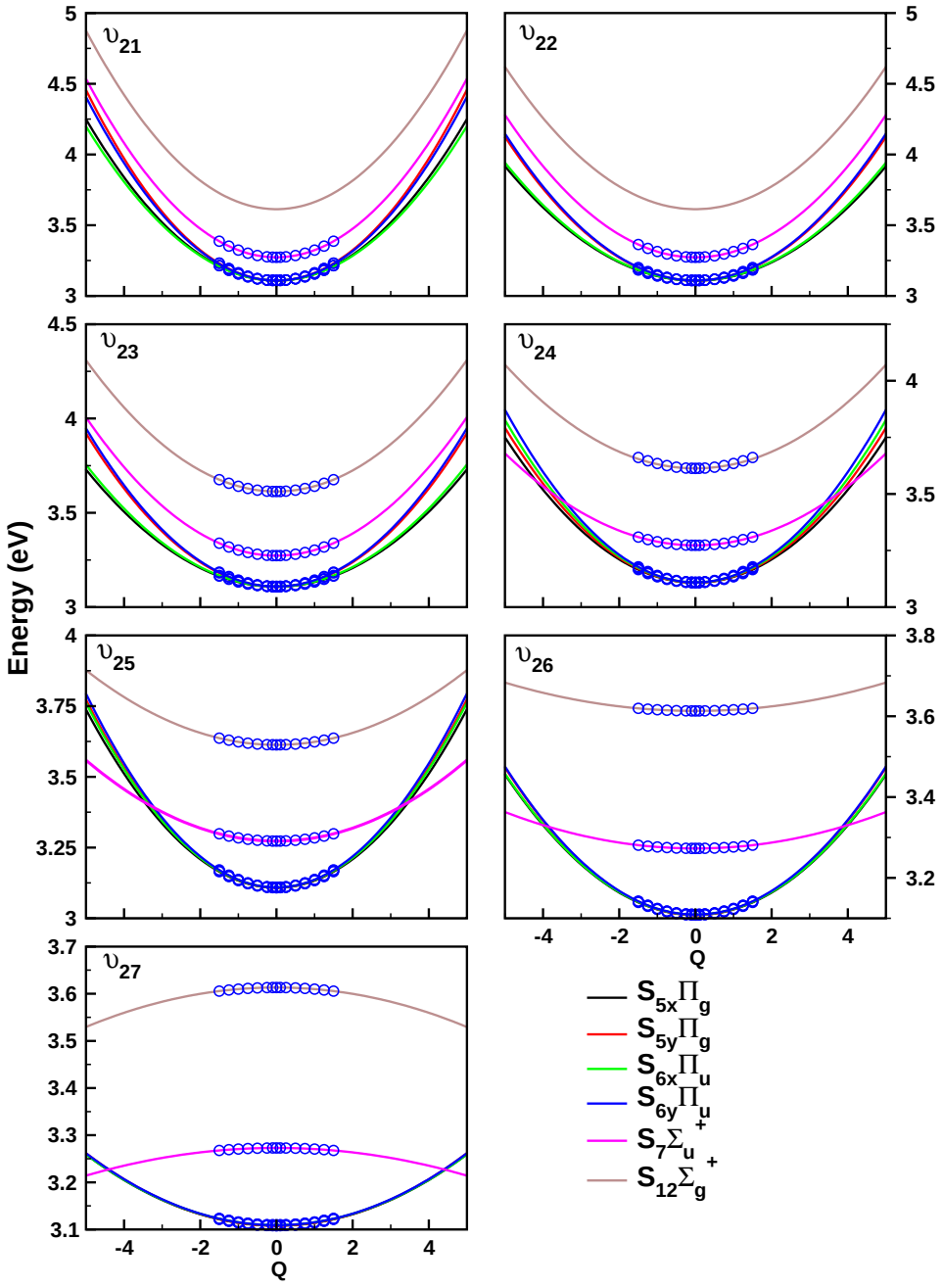

Figure 5.3: Same as Fig. 5.2 for C_{15} along π_u modes.

$$\mathcal{W} = \begin{bmatrix} \mathcal{E}^5 + \frac{1}{2}(\omega_i + \gamma_i^5 + \eta^5)Q_{ix}^2 & 0 & 0 & 0 & 0 & \lambda_i^{5x,12}Q_{ix} \\ 0 & \mathcal{E}^5 + \frac{1}{2}(\omega_i + \gamma_i^5 - \eta_i^5)Q_{ix}^2 & 0 & 0 & 0 & 0 \\ 0 & 0 & \mathcal{E}^6 + \frac{1}{2}(\omega_i + \gamma_i^6 + \eta_i^6)Q_{ix}^2 & 0 & \lambda_i^{6x,7}Q_{ix} & 0 \\ 0 & 0 & 0 & \mathcal{E}^6 + \frac{1}{2}(\omega_i + \gamma_i^6 - \eta_i^6)Q_{ix}^2 & 0 & 0 \\ 0 & 0 & \lambda_i^{6x,7}Q_{ix} & 0 & \mathcal{E}^7 + \frac{1}{2}(\omega_i + \gamma_i^7)Q_{ix}^2 & 0 \\ \lambda_i^{5x,12}Q_{ix} & 0 & 0 & 0 & 0 & \mathcal{E}^{12} + \frac{1}{2}(\omega_i + \gamma_i^{12})Q_{ix}^2 \end{bmatrix} \tag{5.6}$$

This is a $6 \otimes 6$ matrix. By diagonalizing this matrix we will get 6 equations. They are

$$\begin{aligned} V_1 &= \mathcal{E}^5 + \frac{1}{2}(\omega_i + \gamma_i^5 - \eta_i^5)Q_{ix}^2 \\ V_2 &= \mathcal{E}^6 + \frac{1}{2}(\omega_i + \gamma_i^6 - \eta_i^6)Q_{ix}^2 \\ V_{3\pm} &= \frac{\mathcal{E}^5 + \mathcal{E}^{12}}{2} + \frac{2\omega_i + \gamma_i^5 + \eta_i^5 + \gamma_i^{12}}{4}Q_{ix}^2 \pm \sqrt{\left(\frac{\mathcal{E}^{12} - \mathcal{E}^5}{2} + \frac{\gamma_i^{12} - \gamma_i^5 - \eta^5}{4}Q_{ix}^2\right)^2 + (\lambda^{5x,12}Q_{ix})^2} \\ V_{4\pm} &= \frac{\mathcal{E}^6 + \mathcal{E}^7}{2} + \frac{2\omega_i + \gamma_i^6 + \eta_i^6 + \gamma_i^7}{4}Q_{ix}^2 \pm \sqrt{\left(\frac{\mathcal{E}^7 - \mathcal{E}^6}{2} + \frac{\gamma_i^7 - \gamma_i^6 - \eta_i^6}{4}Q_{ix}^2\right)^2 + (\lambda_i^{6x,7}Q_{ix})^2} \end{aligned} \tag{5.7}$$

Similarly the adiabatic PESs along π_u modes obtained by the following equations

$$\begin{aligned} V_1 &= \mathcal{E}^5 + \frac{1}{2}(\omega_i + \gamma_i^5 - \eta_i^5)Q_{ix}^2 \\ V_2 &= \mathcal{E}^6 + \frac{1}{2}(\omega_i + \gamma_i^6 - \eta_i^6)Q_{ix}^2 \\ V_{3\pm} &= \frac{\mathcal{E}^5 + \mathcal{E}^7}{2} + \frac{2\omega_i + \gamma_i^5 + \eta_i^5 + \gamma_i^7}{4}Q_{ix}^2 \pm \sqrt{\left(\frac{\mathcal{E}^7 - \mathcal{E}^5}{2} + \frac{\gamma_i^7 - \gamma_i^5 - \eta^5}{4}Q_{ix}^2\right)^2 + (\lambda^{5x,7}Q_{ix})^2} \\ V_{4\pm} &= \frac{\mathcal{E}^6 + \mathcal{E}^{12}}{2} + \frac{2\omega_i + \gamma_i^6 + \eta_i^6 + \gamma_i^{12}}{4}Q_{ix}^2 \pm \sqrt{\left(\frac{\mathcal{E}^{12} - \mathcal{E}^6}{2} + \frac{\gamma_i^{12} - \gamma_i^6 - \eta_i^6}{4}Q_{ix}^2\right)^2 + (\lambda_i^{6x,12}Q_{ix})^2} \end{aligned} \tag{5.8}$$

Since we found quadratic RT coupling parameters are very small and do not induce a new minimum, here we neglect them in Eq. 5.7

$$V_{3-} = \frac{\mathcal{E}^1 + \mathcal{E}^4}{2} + \frac{1}{2}\omega Q_x^2 \pm \sqrt{\left(\frac{\mathcal{E}^4 - \mathcal{E}^1}{2}\right)^2 + (\lambda^{1x,4} Q_x)^2}$$

Differentiation of V_{3-} with respect to Q_x, yield a minimum at

$$Q_x = \sqrt{\left(\frac{(\lambda^{1x,4})^2}{\omega^2} - \left(\frac{\mathcal{E}^4 - \mathcal{E}^1}{2\lambda}\right)^2\right)}$$

provided the following condition is satisfied

$$2(\lambda^{(1x,4)})^2 > \omega(\mathcal{E}^4 - \mathcal{E}^1).$$

5.5 Absorption spectrum

Vibronic energy levels of the $S_5{}^1\Pi_g$, $S_6{}^1\Pi_u$, $S_7{}^1\Sigma_u^+$ and $S_{12}{}^1\Sigma_g^+$ electronic states of C_{15} are shown and discussed here. These are calculated by the quantum mechanical methods described in Chapter 2 using the parameters of Tables 5.3-5.4. To start with, we construct various reduced dimensional models and examine the vibrational energy levels of each of these electronic states by excluding the PJT coupling with their neighbors. These results help us to understand the role of various vibrational modes and electronic states in the complex vibronic structures of C_{15}. The final simulation of nuclear dynamics is, however, carried out by including all relevant couplings of the Hamiltonian and propagating wave packets using the MCTDH suite of programs [12–15] to elucidate the nonadiabatic coupling effects on the spectral envelopes. The theoretical results are finally compared with the available experimental absorption spectrum of C_{15} [34].

In the uncoupled states situation and in absence of any intermode coupling terms, the Hamiltonian for the $S_5{}^1\Pi_g$ and $S_6{}^1\Pi_u$ states are separable in terms of the σ_g^+, π_g and π_u vibrational modes. One can therefore calculate partial spectra separately for the σ_g^+, π_g and π_u and convolute them to generate the complete spectrum, for these degenerate electronic states. Such a separation reduces the dimension of the secular matrix and facilitates the numerical computation. The vibronic energy level spectrum of the $S_5{}^1\Pi_g$ electronic state is shown in Fig. 5.4. The partial spectra of σ_g^+, π_g and π_u vibrational modes are shown in panels a and b, respectively. The results of convolution of the three partial spectra are shown in panel c. The vibronic energy eigenvalues are obtained by diagonalizing the Hamiltonian matrix using the Lanczos algorithm [42] and are shown as the stick lines in the figure. The envelopes are obtained by convoluting these stick lines with a Lorentzian function with a FWHM of 10 meV. Further details of the calculations are given in Table 5.6. The partial spectrum of the π_g and π_u (panel b) is essentially structureless because of their weak RT coupling (Since RT coupling is quadratic and

weak, it is expected not to contribute much to the spectrum except giving a small shift to the energies). The vibrational modes (panel a), ν_1-ν_7 form progressions and the peaks are ∼2197, ∼2050, ∼2010, ∼1739, ∼1306, ∼819 and ∼282 cm^{-1}, respectively spaced in energy corresponding to the frequencies of these vibrational modes (cf., Table 5.3). The vibrational modes ν_2 and ν_3 forms dominant progression in the band. Very weak fundamental transition due to the bending modes is observed in the spectrum of π_g and π_u modes.

Similar spectra for the RT split $S_6{}^1\Pi_u$ electronic manifold of C_{15} are shown in Fig. 5.5 (a-c). The coupling parameters (see Table 5.3) suggests the vibrational progressions in the $S_6{}^1\Pi_u$ electronic state are very similar to the $S_5{}^1\Pi_g$ electronic state. The vibrational modes ν_2 and ν_3 forms dominant progressions with energy spacings ∼2045 and ∼2007 cm^{-1}, respectively. The excitations from the bending (π_g and π_u) modes is very weak.

The vibrational structure of the S_7 electronic state in absence of coupling with its neighboring states is shown in panel a and the resolved 355 nm experimental recording of Ref [34] is shown in panel b of Fig. 5.6. It can be seen in comparison that the theoretical results are in very good agreement with the experimental band structure of the S_7 state. From the data given in Table 5.3, the excitation of vibrational modes ν_3, ν_4 and ν_5 can be expected in this band. The excitation of the ν_3, ν_5 modes is stronger than that of ν_4. Line spacings of ~ 607, ~ 429 and ~ 288 cm^{-1} corresponding to the frequency of these modes, respectively, are extracted from the theoretical spectrum. Similarly, the spectrum of $S_{12}{}^1\Sigma_g^+$ electronic state is shown in Fig. 5.7 reveals progressions ∼286 and ∼816 cm^{-1} along the vibrational modes ν_6 and ν_5, respectively.

So far we did not consider the PJT coupling of various electronic states in the numerical calculations. On inclusion of this coupling, the separation of the Hamiltonian in terms of the symmetric and degenerate vibrational modes for the degenerate electronic states as explored above is no longer possible. It is therefore necessary to follow the nuclear dynamics simultaneously on six coupled electronic states (four from the two RT split S_5 and S_6 states plus two non degenerate S_7 and S_{12} electronic states) including all relevant vibrational degrees of freedom. Computationally, it turns out to be a daunting task to simulate the nuclear dynamics quantum mechanically by the matrix diagonalization approach employed above. We therefore resort to the MCTDH algorithm [12–15], and propagate WPs on six coupled electronic states including all vibrational degrees of freedom in order to arrive at the desired goal. Even with MCTDH, simulations with 40 vibrational modes is not possible. By looking at the coupling strength of the vibrational modes in Tables 5.3 and 5.4, it is clear that, not all the vibrational modes are important in the nuclear dynamics simulations. We selected thirty vibrational modes (including x and y components of the degenerate vibrational modes) on the basis of the coupling strength. The thirty vibrational degrees of freedom are grouped into four three dimensional particles. The combination scheme of the vibrational modes is given in Table 5.7, along with the sizes of the primitive and SPF bases. The parameters documented in Table 5.7 are optimally chosen to ensure the numerical convergence of the vibronic bands shown in Fig. 5.8. The WP in each calculation is propagated for 200 fs. Fig. 5.8 displays the present theoretical absorption bands of C_{15} in the energy range ∼3-4 eV. The theoretical results of 5.8 are obtained by including the coupling

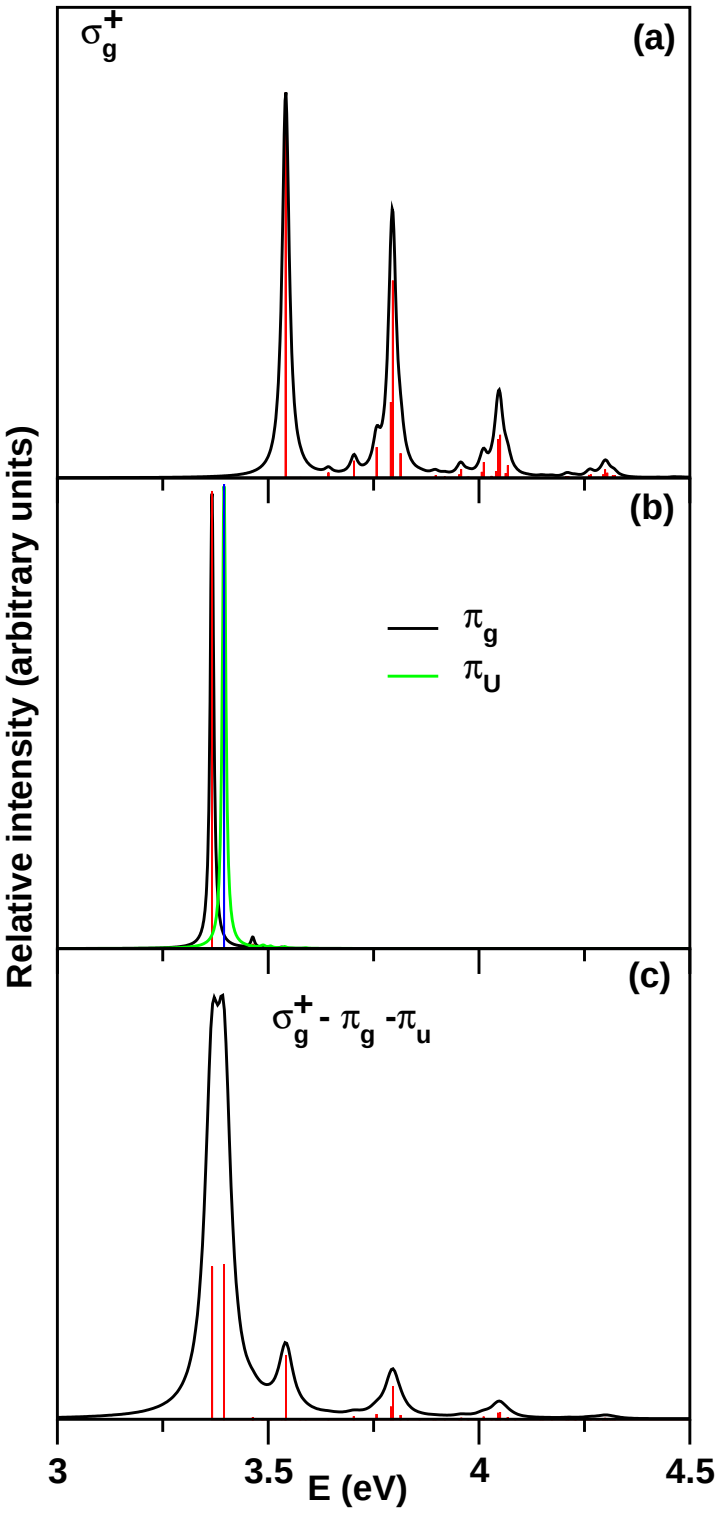

Figure 5.4: The stick vibronic spectra and their convoluted envelopes for the $S_5{}^1\Pi_g$ electronic state of C_{15} calculated with σ_g^+, π_g and π_u modes (indicated in the panel) plotted in panels a and b respectively. The composite spectrum of $S_5{}^1\Pi_g$ by including all the above modes is given in panel c.

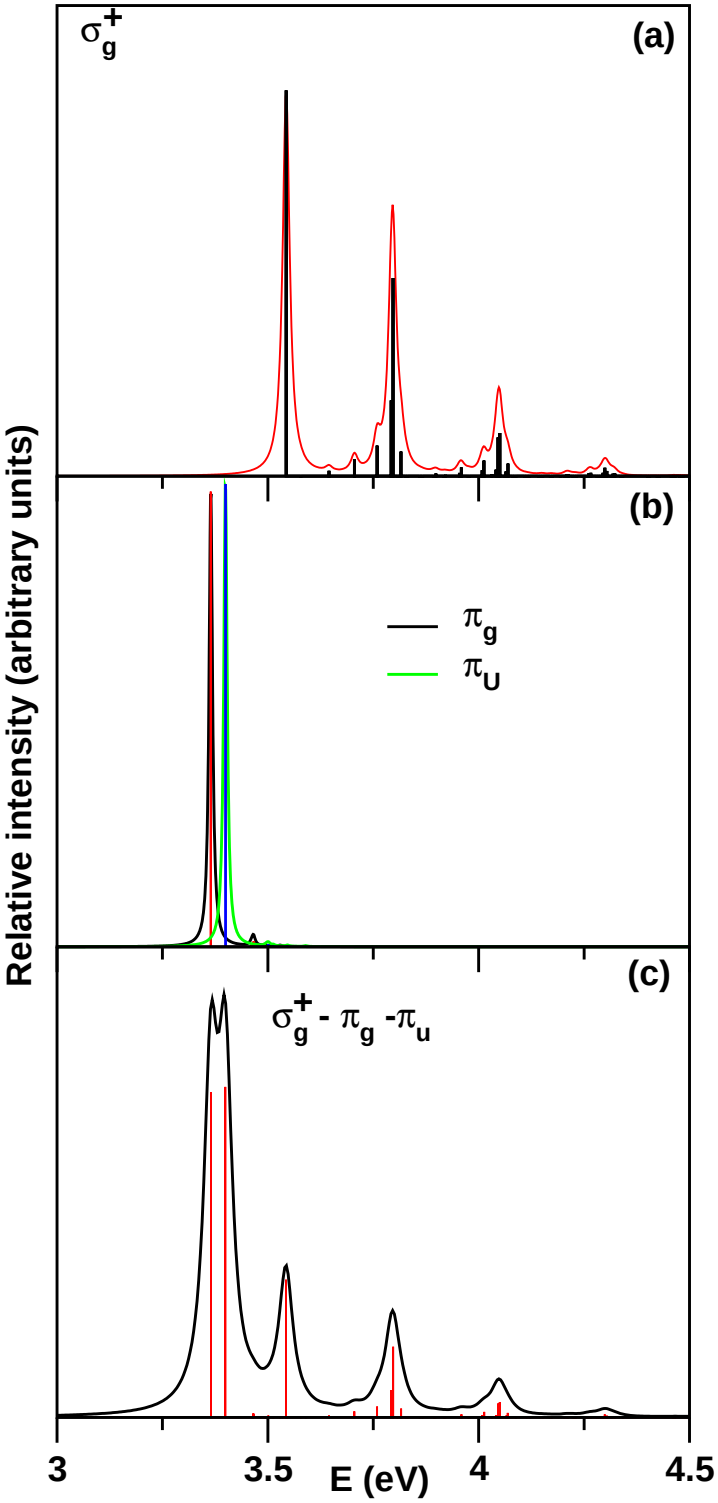

Figure 5.5: Similar as Fig. 5.4 for $S_6{}^1\Pi_u$ electronic state.

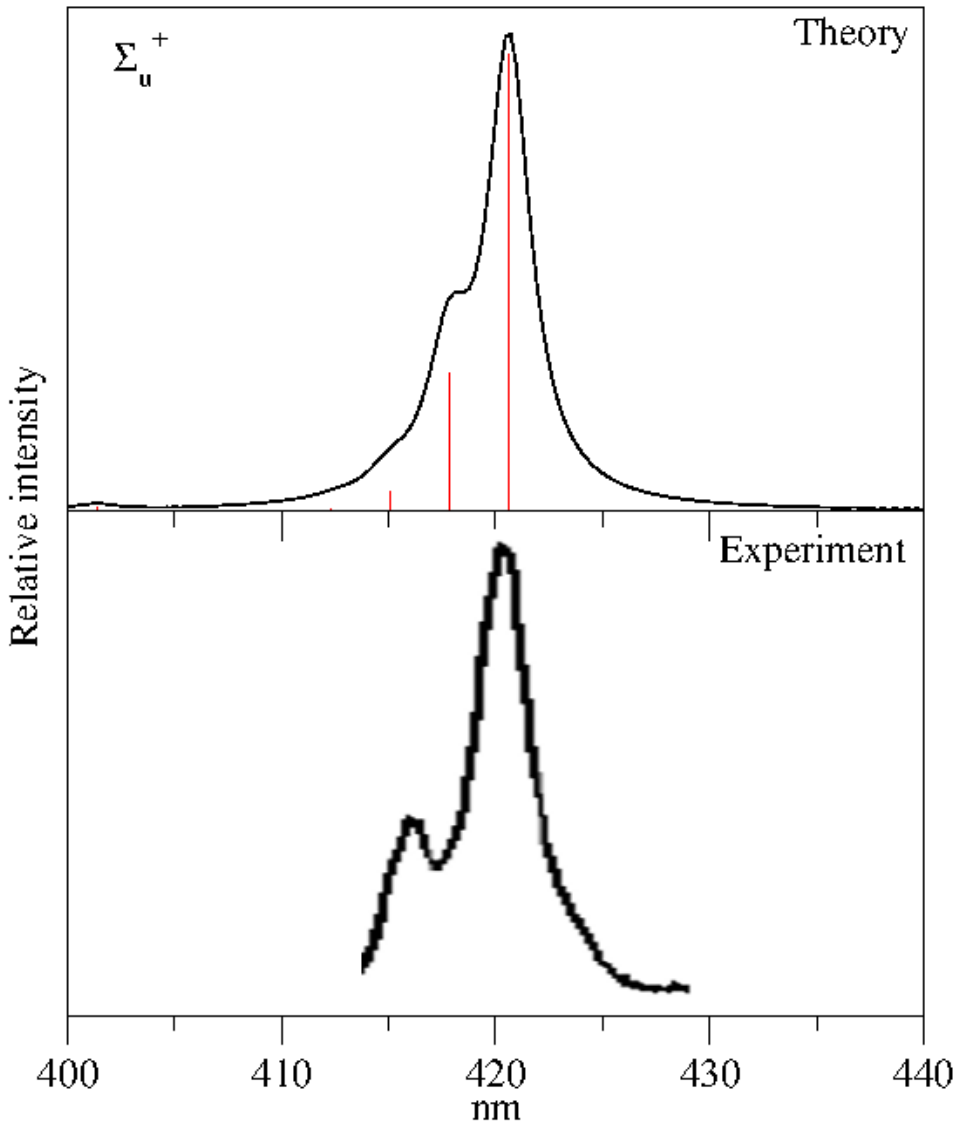

Figure 5.6: The stick vibronic spectrum and the convoluted envelope of the $S_7\,^1\Sigma_u^+$ electronic state of C_{15} calculated with the σ_g^+ vibrational modes plotted in panel a. The 355 nm experimental spectrum is reproduced from Ref. [34] and shown in panel b.

among the states. Six WP propagations in the coupled S_5 -S_6 -S_7 -S_{12} electronic manifold are carried out by initially preparing the WP separately on each of the component state of this manifold. Finally, results from these six calculations are combined. The resulting time autocorrelation function is damped with an exponential function $e^{\frac{-t}{\tau}}$ with τ=66 fs (which corresponds to a 20 meV FWHM Lorentzian function) before Fourier transformation to generate the spectral envelopes of Fig. 5.8.

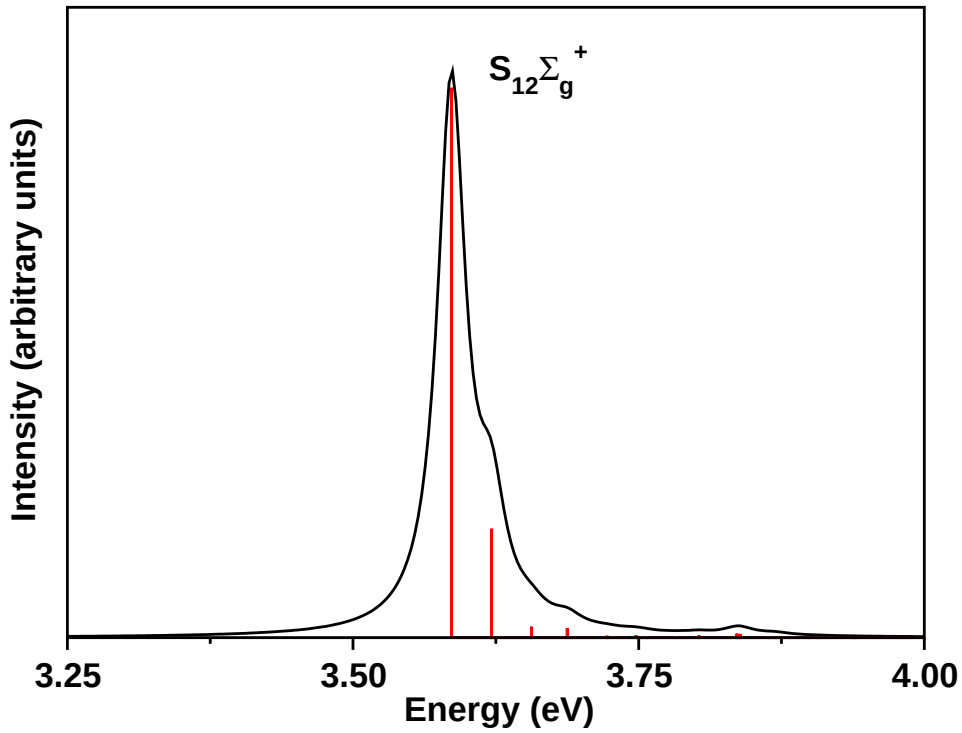

Figure 5.7: Same as Fig. 5.6 for electronic state $S_{12}{}^1\Sigma_g^+$.

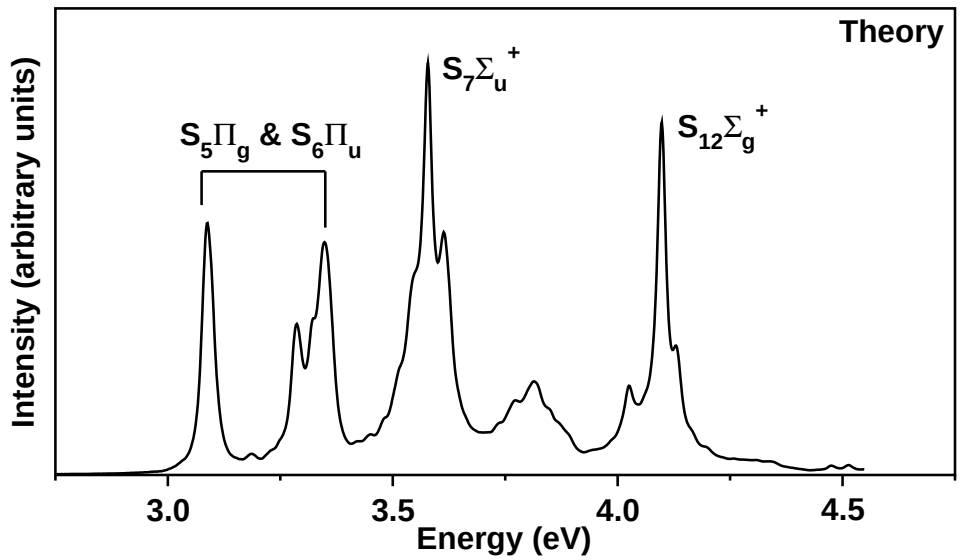

Figure 5.8: The absorption bands of C_{15} obtained from the coupled state dynamics study (see text for details). The intensity in arbitrary units is plotted as as function of the energy of the final vibronic states.

Table 5.6: The number of HO basis functions along with the vibrational mode and the dimension of the secular matrix used in the calculation of the stick vibronic spectra shown in various figures noted below.

Vibrational modes	No. of HO basis	Dimension of secular matrix	Figure(s)
ν_1, ν_2,ν_3,ν_4,ν_5,ν_6,ν_7	8,25,15,8,8,4,4	3072000	5.4 (a)
ν_{15},ν_{16},ν_{17},ν_{18}	8,8,8,8	16777216	5.4 (b)
ν_{21},ν_{22},ν_{23},ν_{24}	8,8,8,8	16777216	5.4 (b)
ν_1, ν_2,ν_3,ν_4,ν_5,ν_6,ν_7	8,25,15,8,8,4,4	3072000	5.5 (a)
ν_{15},ν_{16},ν_{17},ν_{18}	8,8,8,8	16777216	5.5 (b)
ν_{21},ν_{22},ν_{23},ν_{24}	8,8,8,8	16777216	5.5 (b)
ν_1, ν_2,ν_3,ν_4,ν_5,ν_6,ν_7	30,8,8,8,8,8,8	7864320	5.6 (a)
ν_1, ν_2,ν_3,ν_4,ν_5,ν_6,ν_7	30,6,6,6,6,6,6	1399680	5.7

Table 5.7: Normal mode combinations, sizes of the primitive and the single particle basis used in the WP propagation within the MCTDH framework in the six coupled electronic manifold using the complete vibronic Hamiltonian of Eq. (5.2b). First column denotes the vibrational DOF which are combined to particles. Second column gives the number of primitive basis functions for each DOF. Third column gives the number of SPFs for each electronic state.

Normal modes	Primitive basis	SPF basis
ν_1,ν_6,ν_{11},ν_{15y},ν_{16y},ν_{23y}	(6,6,6,6,6,6)	[8,8,8,8,8,8]
ν_2,ν_7,ν_{12},ν_{18x},ν_{17y},ν_{22y}	(6,6,6,6,6,6)	[8,8,8,8,8,8]
ν_3,ν_8,ν_{13},ν_{17x},ν_{v18y},ν_{21y}	(6,6,6,6,6,6)	[8,8,8,8,8,8]
ν_4,ν_9,ν_{14},ν_{16x},ν_{21x},ν_{24x}	(6,6,6,6,6,6)	[8,8,8,8,8,8]
ν_5,ν_{10},ν_{15x},ν_{20x},ν_{23x},ν_{24y}	(6,6,6,6,6,6)	[8,8,8,8,8,8]

5.6 Internal conversion dynamics

As stated in the introduction, the lifetime of the $S_7\,^1\Sigma_u^+$ excited electronic state of C_{15} is of importance for it to qualify as a potential DIB carrier. To be a good carrier for DIBs, the nonradiative decay of the diabatic population of $S_7\,^1\Sigma_u^+$ electronic state is expected [11] be around 70-200 fs. Here in this section, we present the time-dependence of the diabatic electronic populations in the S_5 -S_6 -S_7 -S_{12} electronic states. In order to calculate the latter we recorded the time-dependence of the diabatic electronic populations for an initial transition to each of the above electronic states separately. The results are shown in Fig. 5.9 (a-d). Interesting observations on the dynamical mechanism can be obtained from these population curves in conjunction with the coupling parameters given in Tables 5.3 and 5.4 and the stationary points on the PESs detailed in Section 5.4.

In panel a, the population dynamics is shown for an initial transition of the WP to one of the two RT split components of the $S_5\,^1\Pi_g$ electronic state. In contrast to the well-

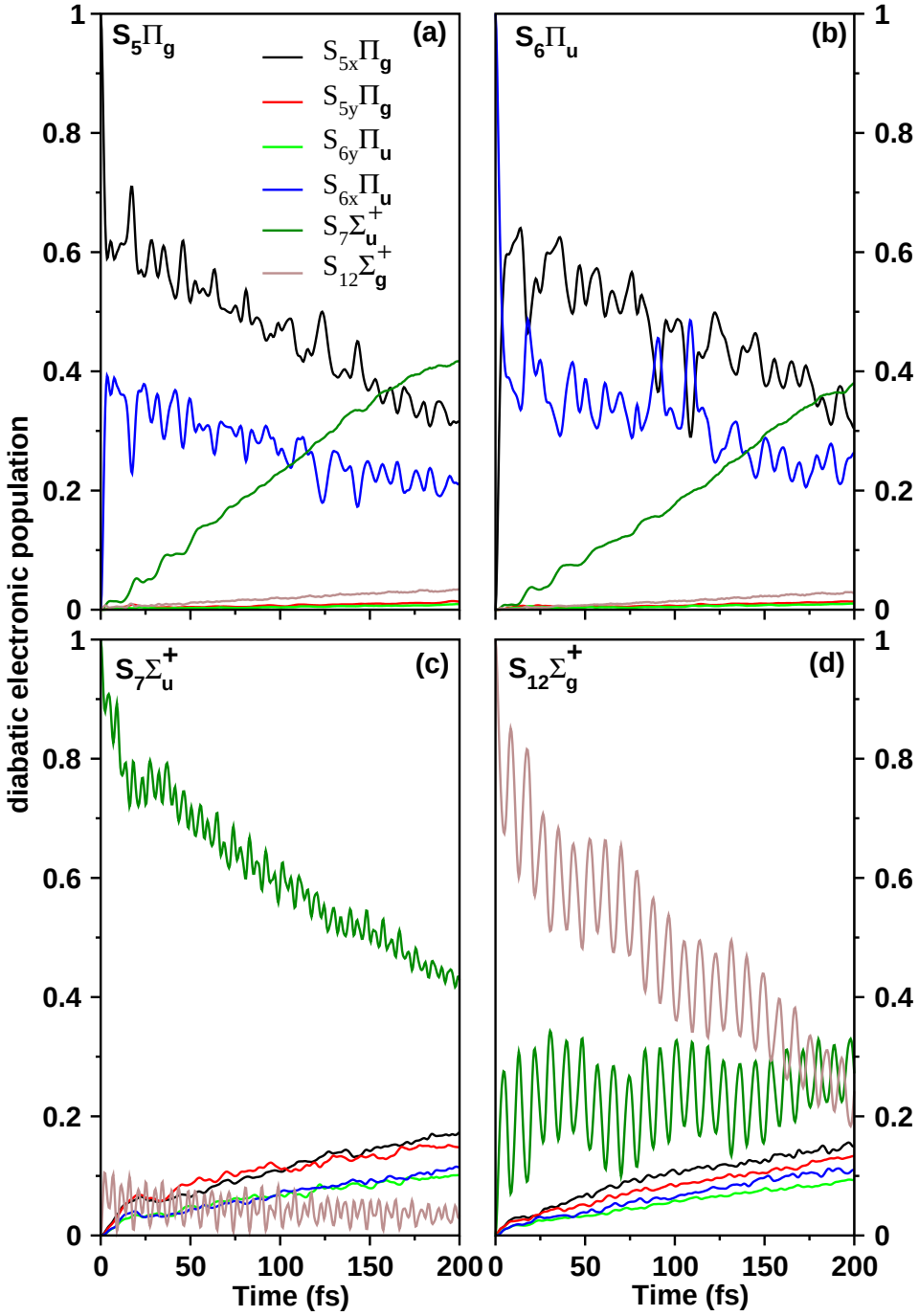

Figure 5.9: The time-dependence of diabatic electronic populations in the S_5 -S_6 -S_7 -S_{12} coupled states nuclear dynamics of C_{15}. The results obtained by initially locating the WP on the x and y components of S_5 and S_6 states and S_7 and S_{12} states are shown in panels (a-d), respectively.

known JT effect where the decay and growth of the population of x and y components of the degenerate electronic can be seen, the population transfer to the counter component is very minimal in the RT case. This is due to the small RT coupling found in the $S_5{}^1\Pi_g$ and $S_6{}^1\Pi_u$ electronic states. The $S_5{}^1\Pi_g$ and $S_6{}^1\Pi_u$ electronic states are coupled by σ_u^+ modes and it can be seen from the Table 5.4 that this coupling is strong along ν_{10} and ν_{11} vibrational modes. From Table 5.5, it can be seen that the location of the energetic minimum of S_5 -S_6 and S_5 -S_7 CIs lie just ∼0.33 eV and ∼0.40 eV above the minimum of the S_5 electronic state. Hence population transfer to S_6 and S_7 state is expected in this case. The decay of population of the x component of S_5 state and the growth of the S_6 (x component) and S_7 state population can be clearly seen from the diagram (panel a). The population of S_{12} electronic state show only minor variations in this case as the minimum of S_5 -S_{12} CIs lie ∼0.84 eV above the minimum of S_5 electronic state and they are weakly coupled. It is therefore clear that the electronic nonadiabatic dynamics in this situation is predominantly governed by the PJT coupling with S_6 and S_7 electronic states. The initial decay of the population of the $S_5{}^1\Pi_g$ state relates to a decay rate of ∼56 fs.

Panel b of Fig. 5.9 portrays the population dynamics when the WP is initially prepared on the x component of S_6 state. The S_5 and S_6 states are nearly degenerate at the vertical configuration. The initial depletion of the diabatic electronic population of S_6 state amounts to a nonradiative decay rate of ∼ 25 fs. It can be seen that the decay of the S_6 population mainly contributes to the growth of the population of x component of the S_5 state and S_7 state. This reflects that the coupling of the S_6 state with S_5 and S_7 states is much stronger (cf., Table 5.4) than the RT coupling within the S_6 state.

The population dynamics of the WP initially prepared on the S_7 is shown in panel c. In this case the electronic diabatic population of S_7 state transfers to S_5 and S_6 electronic states. The decay rate of the S_7 electronic state are estimated to be ∼ 110 fs. This population decay is indeed within the proposed range of ∼70-200 fs [10, 11]. It is already stated that while the PJT coupling between S_5 and S_7 states is strong, the PJT coupling between S_6 and S_7 electronic states is weak. The minimum of S_5 -S_7 and S_6 -S_7 are just ∼0.04 eV above the minimum of S_7 electronic state. Hence the population of the S_7 state is expected to transfer to S_5 state. The S_5 state in-turn coupled strongly to S_6 state via σ_u^+ modes. A population transfer to S_6 state from S_7 state can also be seen.

Finally, the electronic population dynamics for an initial propagation of the WP on S_{12} state is shown in panel d. It can be seen that the S_{12} state decays at a much faster rate ∼ 63 fs compared to the S_7 state. This is due to the relatively stronger PJT coupling between the S_7 -S_{12} states. Only minor population transfer takes place to the S_5 and S_6 coupled electronic manifold in this case

5.7 Summary

A detailed theoretical account of the multimode RT and PJT interactions in some selected electronic states of linear C_{15} cluster is presented here to elucidate the lifetimes of its excited electronic state $S_7{}^1\Sigma_u^+$. The vibronic Hamiltonian is constructed in a diabatic

electronic basis, including the RT coupling within the degenerate S_5 and S_6 electronic states and the PJT couplings of these RT split states with the nondegenerate S_7 and S_{12} electronic states of C_{15}. The coupling parameters of the vibronic Hamiltonian are determined by calculating the adiabatic PESs of the $S_5\,^1\Pi_g$, $S_6\,^1\Pi_u$, $S_7\,^1\Sigma_u^+$ and $S_{12}\,^1\Sigma_g^+$ electronic states along each of the 40 vibrational modes. First principles nuclear dynamics calculations are carried out both via time-independent and time-dependent quantum mechanical methods to simulate the nonadiabatic nuclear motion on the coupled manifold of these electronic states. The theoretical results are found to be in good accord with the available experimental results. The final theoretical simulations using the full Hamiltonian of Eqs. 5.2-5.5b can only be carried out by propagating WPs employing the MCTDH algorithm [12–15]. A careful examination of various theoretical results enabled us to arrive at the following conclusions. The RT effect in the S_5 and S_6 electronic states of C_{15} is very weak. The PJT coupling between the S_5 and S_6 dominates the RT coupling. Due to the clustering of the four excited states within $\sim$ 1.0 eV, the nonradiative processes are found to be dominanting in predicting the vibronic structure and the transfer of diabatic electronic population among these states. The initial decay of the diabatic population of $S_7\,^1\Sigma_u^+$ is estimated to be $\sim$110 fs, which lie in the much anticipated range $\sim$70-200 fs [10, 11].

References

[1] T. P. Snow and B. J. McCall, Annu. Rev. Astron. Astrophys **44**, 367, (2006).

[2] W. H. Smith, T. P. Snow and D. G. York, Astrophys. J. **218**, 124 (1977).

[3] A. E. Douglas. Nature **269** 130 (1997).

[4] W. Huggins, Proc. R. Soc. Landon **33**, 1 (1982); G. Herzberg, Astophys. J. **96**, 314 (1942).

[5] W. Weltner, Jr. and R. J. van Zee, Chem. Rev. **89**, 1713 (1989).

[6] A. V. Orden and R. J. Saykally, Chem. Rev. **98**, 2313 (1998).

[7] J. P. Maier Chem. Soc. Rev. **17**, 45, (1988).

[8] J. P. Maier Chem. Soc. Rev. **26**, 21, (1997).

[9] J. P. Maier J. Phys. Chem. A **102** 3462 (1998).

[10] E. B. Jochnowitz and J. P. Maier, Annu. Rev. Phys. Chem. **59**, 519 (2008).

[11] C. A. Rice and J. P. Maier, J. Phys. Chem. A **117**, 5559 (2013).

[12] G. A. Worth, M. H. Beck, A. Jäckle, and H. -D. Meyer, The MCTDH Package, Version 8.2, (2000), University of Heidelberg, Heidelberg, Germany. H. -D. Meyer, Version 8.3 (2002), Version 8.4 (2007). See http://mctdh.uni-hd.de.

[13] H. -D. Meyer, U. Manthe, and L. S. Cederbaum, Chem. Phys. Lett. **165**, 73 (1990).

[14] U. Manthe, H. -D. Meyer, and L. S. Cederbaum, J. Chem. Phys. **97**, 3199 (1992).

[15] M. H. Beck, A. Jäckle, G. A. Worth, and H. -D. Meyer, Phys. Rep. **324**, 1 (2000).

[16] M. Born and R. Oppenheimer, Ann. Phys. **84**, 457 (1927).

[17] C. J. Ballhausen and A. E. Hansen, Ann. Rev. Phys. Chem. **23**, 15 (1972).

[18] R. Englman, The Jahn-Teller Effect, (Wiley, New York, 1972).

[19] M. Baer, Beyond Born-Oppenheimer:electronic non-adiabatic coupling terms and conical intersections, (John Wiley and Sons, 2006).

[20] H. Köppel, W. Domcke and L. S. Cederbaum, *Adv. Chem. Phys.* **57**, 59 (1984).

[21] S. Mahapatra, Acc. Chem. Res. **42**, 1004 (2009).

[22] Conical Intersections: Electronic Structure, Dynamics and Spectroscopy, edited by W. Domcke, D. R. Yarkony, and H. Köppel (World Scientific, Singapore, 2004).

[23] H. A. Jahn and E. Teller, Proc. R. Soc. London, Ser. A **161**, 220. (1937).

[24] R. Renner, Z. Physik **92**, 172 (1934).

[25] J. A. Pople, Mol. Phys.**3**, 16, (1960).

[26] A. J. Merer and D. N. Travis, Can. J. Phys. **43**, 1795 (1965).

[27] J. A. Pople and H. C. Louguet-Higgins, Mol. Phys. **1**, 372 (1958).

[28] H. Köppel, W. Domcke and L. S. Cederbaum, J. Chem. Phys. **74**, 2945 (1991).

[29] M. Perić, M. Petković and S. Jerosimić, Chem. Phys. **343**, 141 (2008).

[30] M. Perić, R. Ranković and S. Jerosimić, Chem. Phys. **344**, 35 (2008)

[31] I. B. Bersuker, *The Jahn-Teller effect*, (Cambridge University Press, Cambridge (U.K), 2006).

[32] P. Garcia-Fernandez and I. B. Bersuker, Int, Jou, Quant, Chem, **112**, 3025 (2012).

[33] J. M. L. Martin, J. E. Yazal and J-P Francois, Chem. Phys. Lett. **252**, 9, (1996).

[34] D. Forney, P. Freivogel, M. Grutter, and J. P. Maier, J. Chem. Phys. **104**, 4954 (1996);

[35] T. H. Dunning, Jr., J. Chem. Phys. **90**, 1007 (1989).

[36] E. B. Wilson Jr., J. C. Decius and P. C. Cross, *Molecular vibrations* (McGraw-Hill, New York, 1955).

[37] M. J. Frisch, *et al.* Gaussian 03, Revision B. 05, Gaussian, Inc., Pittsburgh, PA, 2003.

[38] H. -J. Werner, P. J. Knowles, R. D. Amos, A. Bernhardsson, and others, MOLPRO-2002, a package of ab initio programs; Universitat Stuttgart: Stuttgart, Germany; University of Birmingham:Birmingham, United Kingdom, 2002.

[39] M. Döscher, H. Köppel, and P. Szalay, J. Chem. Phys. **117**, 2645, (2002)

[40] T. S. Venkatesan, H.-D. Meyer, H. Köppel, L. S. Cederbaum and S. Mahapatra, J. Phys. Chem. A, **111**, 1746, (2007).

[41] T. Mondal, S. R. Reddy and S. Mahapatra, J. Chem. Phys. **137**, 054311 (2012)

[42] J. Cullum and R. Willoughby, Lanczos Algorithms for Large Symmetric Eigenvalue Problems (Birkhäuser, Boston, 1985, Vols. I and II).